Available online at www.sciencedirect.com
SCIENCE DIRECT
Polymer 46 (2005) 12670–12676
polymer
www.elsevier.com/locate/polymer

Preparation and characterization of a PMMA/$Ce(OH)_3$, Pr_2O_3/graphite nanosheet composite

Zunli Mo [a,b,*], Yinxia Sun [a], Hong Chen [a], Ping Zhang [a], Dandan Zuo [a], Yanzhi Liu [a], Hejun Li [b]

[a] College of Chemistry and Chemical Engineering, Northwest Normal University, Lanzhou 730070, People's Republic of China
[b] College of Material Science and Engineering, Northwestern Politechnical University, Xi'an 710072, People's Republic of China

Received 4 July 2005; received in revised form 9 October 2005; accepted 25 October 2005
Available online 10 November 2005

Abstract

An easy process for the synthesis of poly(methyl methacrylate)/$Ce(OH)_3$, Pr_2O_3/graphite nanosheet (PMMA/$Ce(OH)_3$, Pr_2O_3/NanoG) composite was developed. Graphite nanosheets (NanoG) were prepared by treating the expanded graphite with sonication in aqueous alcohol solution. The PMMA/$Ce(OH)_3$, Pr_2O_3/NanoG composites were prepared via in situ polymerization of MMA monomer in the presence of graphite nanosheets and $Ce(OH)_3$, Pr_2O_3 through reverse micelle template, in which the methyl methacrylate was designated as the oily phase. The composites were then dispersed with chloroform and coated on glass slides to form films. Scanning and transmission electron microscopy were used to characterize the structure and dispersion of the graphite nanosheets and the composites. The results showed that the high-aspect-ratio structure of the nanosheets played an important role in forming a conducting network in the PMMA matrix. From thermogravimetric analysis, the introduction of graphite nanosheets and inorganic nanopartices exhibited a beneficial effect on the thermal stability of PMMA.

Keywords: Composites; Graphite nanosheet (NanoG); $Ce(OH)_3$–Pr_2O_3

1. Introduction

Graphite is layered crystal with a *c*-axis lattice constant of 0.66 nm. Carbon atoms within a layer are covalently bonded, while layers are bound by much weaker van der Waals forces. It is frequently used especially for an improvement of electrical conductivity, antistatic properties as well as thermal conductivity of plastics. Polymer/graphite composites have long been used in conducting, aerospace and electrochemistry fields [1–6]. However, it is rather difficult to prepare the conductive graphite/polymer composites via direct intercalation method [7–9]. Simultaneity, finding a convenient method for preparation of a composite with excellent physical properties, in which graphite particles disperse homogeneously in a continuous polymer matrix, is always an interesting project in the material science. Generally, it is difficult to be fulfilled due to their incompatibility. Thus, it is important to improve the incompatibility between graphite and polymer. It is generally needed to achieve nanoscale dispersion of graphite in polymer matrix with certain chemical or physical modification to the graphite [9,10]. Expanded graphite (EG) is composed of a large number of delaminated graphite sheets and its electrical conductivity is not obviously affected compared with the original graphite flake [11–13]. In this sense, monomers and polymers can be intercalated into the pores and layers of the expanded graphite (EG) to form conductive composite. Hence, polymer/expanded graphite composites with low percolation threshold of conductivity and highly thermal storage properties have been disclosed [8,14–16]. For these composites, however, the monomers and polymers might not be able to diffuse into the closed cavities inside the expanded graphite (EG), owing to lots of graphite sheets on expanded graphite (EG) firmly interlock with each other. The aggregates may also result from the inadequate intercalation of monomers or polymer in solution into the space between graphite layers. Moreover, since some pores are closed in nature, no monomers or polymer solution is expected to be able to penetrate into them. As a result, the graphite sheets around such pores might not be separated by polymer, but will overlap each other forming the aggregates during processing.

* Corresponding author. Address: College of Chemistry and Chemical Engineering, Northwest Normal University, Lanzhou 730070, People's Republic of China. Tel.: +86 931 7971829; fax: +86 931 7971933.
E-mail address: mozl@163.com (Z. Mo).

0032-3861/$ - see front matter © 2006 Elsevier Ltd. All rights reserved.
doi:10.1016/j.polymer.2005.10.117

Generally, relatively high loading level of graphite within a conductive polymeric composite is needed to afford a satisfactory conductivity and to reach the critical percolation value, as the graphite particle size is at micrometer and millimeter scales. However, too high loading level of the conductive filler could generally lead to the poor mechanical properties and high density of the materials [17,18]. In order to develop a conducting network within polymer matrix with fewer filler, one could consider using nanoscale fillers as conducting charges. When nanoscale conducting fillers is dispersed in polymer matrix, the particular morphology and structure developed provides the advantage in forming the conducting network. In attempt to achieve homogeneous nanodispersion of graphite in polymer matrix, we proposed delamination of graphite nanosheets via powdering the expanded graphite [8,19–21]. More recently, graphite nanosheets were used to prepare polymer/graphite nanosheets composites via in situ polymerization [19–22]. Nevertheless, there is no report on the polymer/inorganic nanoparticles/graphite nanosheets composites up to now.

In this study, the expanded graphite was firstly powdered to make graphite nanosheets with sonication in aqueous alcohol solution. Then PMMA/$Ce(OH)_3$, Pr_2O_3/NanoG composites were prepared via in situ polymerization of MMA monomer in the presence of graphite nanosheets and $Ce(OH)_3$, Pr_2O_3 through reverse micelle template, where the graphite nanosheets were dispersed homogeneously. The morphology, thermal properties and electrochemical properties of the composites were also investigated based on scanning electron microscope (SEM), transmission electronic microscopy (TEM), Fourier transform infrared (FTIR), and thermogravimetric analysis (TG-DTA).

2. Experimental

2.1. Materials

The graphite used in this study was expandable graphite, supplied from Shandong Qingdao Graphite Company (Qingdao, China). The methyl methacrylate (MMA) monomer and $CHCl_3$ (AR, Beijing Chemical Reagent Co., China) were purified by vacuum distillation before use. The initiator, 2,2′-azobis (isobutyronitrile) (AIBN) was bought from the First Shanghai Chemical Reagent Plant, and purified by recrystallization from its ethanol solution. Concentrated hydrochloric acid, pentaerythritol, NaOH, $Pr_2(CO_3)_3$, $Ce_2(CO_3)_3$ and cetyltrimethylammonium bromide (CTAB), were of analytical grade and used as received.

2.2. Preparation of graphite nanosheets

The dried expandable graphite powders were heat treated at 1050 °C for 15 s to obtain expanded graphite particles (or called graphite worm). The expansion ratio was about 300. The expanded graphite was finally dispersed in a 75 wt% alcohol solution and sonicated for 12 h, then filtrated and washed completely with distilled water. The obtained graphite powders, which were called graphite nanosheets, were dried under vacuum at ambient temperature for 24 h.

2.3. Preparation of PMMA/Pr_2O_3, $Ce(OH)_3$/NanoG composite and its films

PMMA/Pr_2O_3, $Ce(OH)_3$/NanoG composites were prepared using the following procedure. Certain amount of $Pr_2(CO_3)_3$, $Ce_2(CO_3)_3$ was dissolved in hydrochloric acid to form 1.0 mol/L $PrCl_3$, $CeCl_3$ aqueous solution. Firstly, 1.0 g CTAB, 15.0 mL MMA, 3.0 mL 1.0 mol/L $PrCl_3$, $CeCl_3$ aqueous solution and a little pentaerythritol were mixed. The mixture was sonicated under nitrogen atmosphere at room temperature for 15 min. Secondly, added 0.05 g nanosheets into the mixture and sonicated for another 15 min. Thirdly, 3.0 mL 3.0 mol/L NaOH aqueous solution was added into the mixture and treated for 30 min at the same terms. Then, the mixture was treated for 3 h at 60 °C followed by addition of 0.075 g 2,2′-azobis (isobutyronitrile). Finally, the resulting was dispersed with $CHCl_3$ and coating the dispersion on glass slides made the conducting films.

2.4. Characterization and measurements

Scanning electron microscope (SEM; JEOL, JSM-6330F) was used to observe the morphologies of graphite nanosheets. Prior to SEM examination, the specimens were coated with a very thin layer of Au. Transmission electron microscopy (TEM) was performed with a JEOL100CX-II model transmission electron microscope at 100 kV accelerated voltage. The observations were carried out after retrieving the slices onto Cu grids. Fourier transforms infrared (FTIR) spectra of the composites in KBr pellets were recorded on an EQUINOX55 FTIR spectrometer (Bruker). The weight loss temperatures of the composites were determined with a Perkin–Elmer thermogravimetric analyzer (TG-DTA; model SSC-5200) from 20 to 900 °C under environment atmosphere (10 °C/min).

3. Results and discussion

3.1. Structure of graphite nanosheets

We sonicated the expanded graphite in alcohol solution to gain shiny graphite powder. Fig. 1 showed the SEM image of sonicated expanded graphite. It revealed that the expanded graphite was tore to sheets with thickness of 30–80 nm and a diameter of 0.5–20 μm named graphite nanosheets. The prepared graphite nanosheets possessed a high aspect ratio (width-to-thickness) of around 100–500. The powder had an apparent density of 0.015 g/cm^3, much smaller than that of the original flake graphite, 2.25 g/cm^3. The result was similar to that reported by other researchers [21,23,24], e.g. Fukuda et al. [25] also treated expanded graphite with sonication and found that graphite sheets existed as separated nanosheets with the thickness of about 70 nm. It substantiated that the expanded graphite were composed of graphite nanosheets. Such

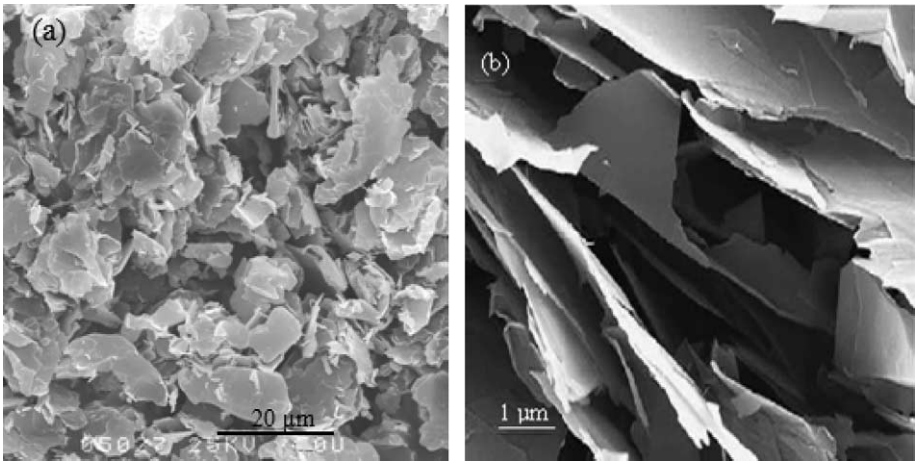

Fig. 1. SEM of graphite nanosheets: (a) lower magnification and (b) higher magnification.

nanoscale dispersion facilitated the formation of the electrical conductive network in the polymer matrix at very low filler loading.

The more detailed structure of graphite nanosheets was examined by TEM technique. Fig. 2 showed that the graphite nanosheets consisted of thinner graphite nanolamella with thickness of 1–5 nm or thinner and with the space of about 5 nm. The result was similar to that reported by other researchers [26]. The gallery space in the nanosheets as well as the contorted structure of the nanosheets might be the contribution factors to the low apparent density of the graphite nanosheet powder. Selected area diffraction (SAD) also showed that the graphite nanosheet was no longer single crystal structure [8,19,20].

3.2. Structure of PMMA/Pr_2O_3, $Ce(OH)_3$/NanoG composite and its films

Graphite nanosheets, like other kinds of nanoparticles, tended to accumulate each other and were difficult to be dispersed in polymer by traditional ways as blending on twin-roller. Sonication was an effective way for the optimal dispersion of the graphite nanosheets in reverse micelle system and in the polymer matrix. And the methyl methacrylate was designated as oily phase and the inorganic particles aqueous solution as water phase in the reverse micelle system depending on cetyltrimethylammonium bromide. With the 2,2′-azobis (isobutyronitrile) adding, an instant in situ polymerization of the methyl methacrylate occurred and then the graphite nanosheets and inorganic nanoparticles were dispersed and fixed among the polymer molecules. The chemical reaction we employed for the preparation of inorganic nanoparticles Pr_2O_3 and $Ce(OH)_3$ could be formulated as [27]:

$$2PrCl_3 + 6NaOH = Pr_2O_3 \cdot 3H_2O + 6NaCl$$

$$CeCl_3 + 3NaOH = Ce(OH)_3 + 3NaCl$$

Thus, the nanodispersion composites could be successfully obtained. The resulting was then dispersed with $CHCl_3$ and the conducting films were made by coating the dispersion on glass slides. The process of the formation of composite of PMMA/Pr_2O_3, $Ce(OH)_3$/NanoG composite could be described more clearly by a schematic illustration in Fig. 3.

Fig. 4(a) and (b) showed the typical SEM image of PMMA/Pr_2O_3, $Ce(OH)_3$/NanoG composites and the composites thin films. We could observe clearly from Fig. 4(a) that graphite nanosheets dispersed in PMMA matrix and the PMMA also embedded within the nanospace inside the NanoG, the graphite nanosheets were distributed quite uniformly within the PMMA matrix and no aggregates of the graphite particles could be seen in the mixture, and then the inorganic nanoparticles Pr_2O_3 and $Ce(OH)_3$ were covered in the PMMA matrix and graphite

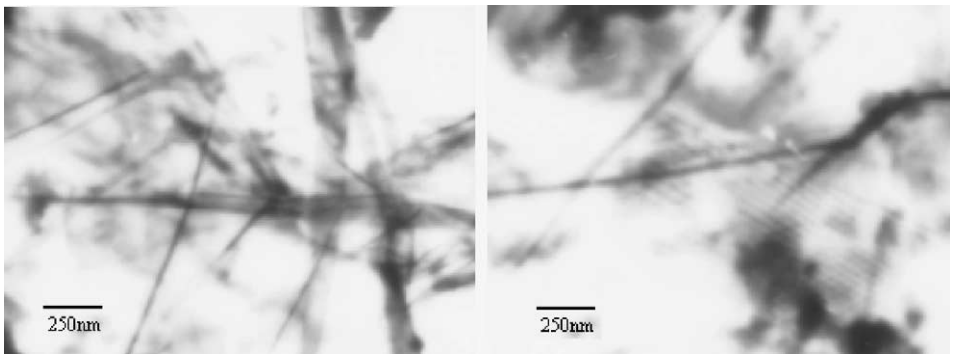

Fig. 2. TEM of graphite nanosheets.

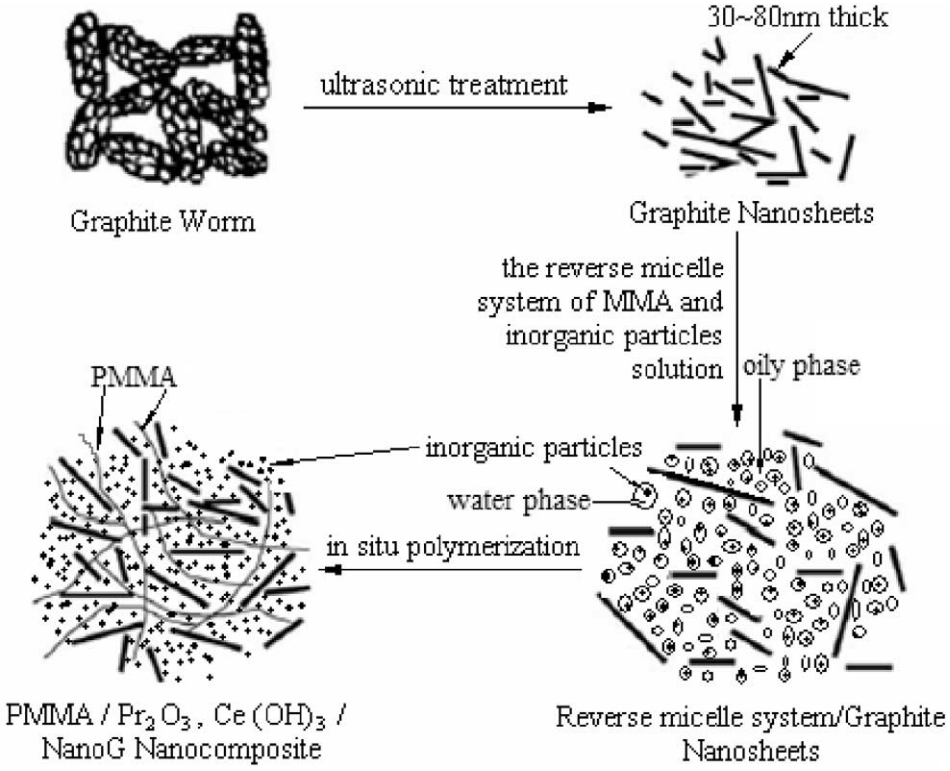

Fig. 3. Schematic illustration the formation of PMMA/Pr_2O_3, $Ce(OH)_3$/NanoG composite via in situ polymerization.

mixture separately. Obviously, such a granular structure was in favor for increasing the interfacial affinity of inorganic nanoparticles and graphite nanosheets with the matrix and leading to an ensured electrical contact. The composite showed the signs of internal porosity in Fig. 4(a). The internal porosity mainly originated from the evaporation of the water dripping in the reverse micelle in the course of the composite dryness.

Fig. 4(b) was the SEM of the composite thin films. The composites showed a uniform distribution of small inorganic nanoparticles in graphite nanosheets and PMMA matrix. It was apparent that PMMA/Pr_2O_3, $Ce(OH)_3$/NanoG composites formed a continuous and relative system. The film structure seen in Fig. 4(b) were similar to the composite, unlike the composite, however, the film had no porosity in their inner. Thus, from the SEM image of the composite material, we concluded that inorganic nanoparticles were separated by alternating organic polymer and graphite nanosheets mixture in the composites.

Fig. 5 was a typical TEM micrograph of PMMA/Pr_2O_3, $Ce(OH)_3$/NanoG composite. The gray lines were the graphite nanosheets, and the dark spot represented the inorganic nanoparticles in the cross section of PMMA/Pr_2O_3, $Ce(OH)_3$/NanoG composite, in which the fine and relatively uniform inorganic nanoparticle size was in the range of 50–80 nm. It was apparent that the nanoscale patterns of strips considered

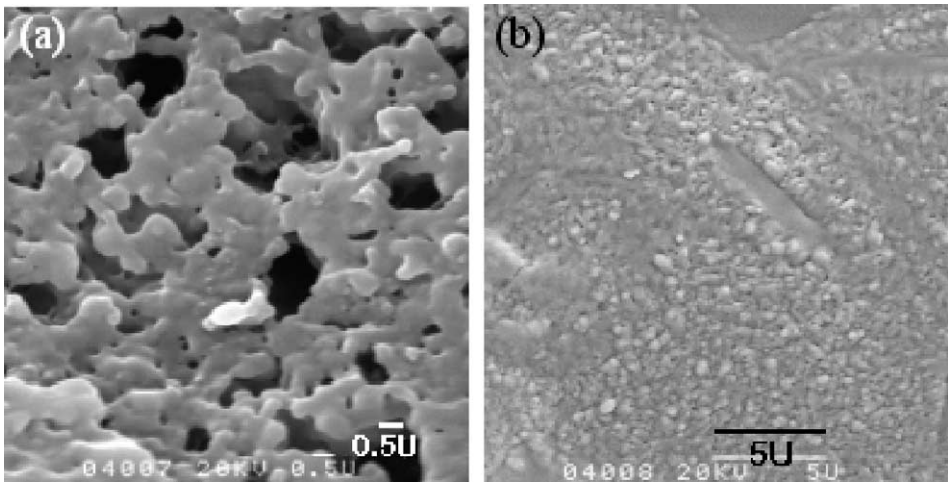

Fig. 4. SEM image of PMMA/Pr_2O_3, $Ce(OH)_3$/NanoG composite (a) and the composite thin films (b).

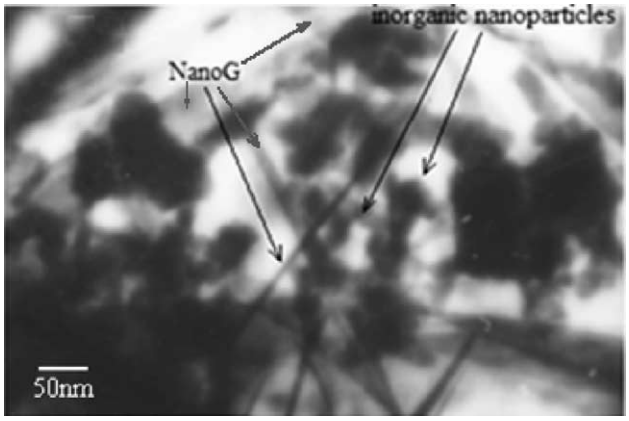

Fig. 5. TEM micrograph of PMMA/Pr_2O_3, $Ce(OH)_3$/NanoG composite.

the nanoscale dispersion of the graphite nanosheets and inorganic nanoparticles within PMMA matrix. Graphite sheets as observed had thickness of 10–40 nm and the average length of about 450 nm, indicating a large aspect ratio (width-to-thickness), which facilitates to yield the conductive network within the matrix. The conductive network was believed to lead to the greatly improved electrical conductivity for the composite. Such nanoscale dispersion endowed the advantages in formation of the electrical conductive network in the polymer matrix at very low filler loading. This figure revealed a fine and relatively uniform inorganic nanoparticle size in the range of 50–80 nm.

Fig. 6 showed the FT-IR absorption spectra of the PMMA/Pr_2O_3, $Ce(OH)_3$/NanoG composite. The peak at 3440.71 and 1389.42 cm^{-1} could be attributed to hydroxyl (–OH) stretching vibrations of graphite nanosheets or the binding water symmetrical stretching vibrations and deformation vibrations of hydroxyl (O–H) in the PMMA/Pr_2O_3, $Ce(OH)_3$/NanoG composites. The peak at 1731.53 cm^{-1} was reduced to the C=O stretching vibrations of the PMMA and the graphite nanosheets. This was consistent with another report [28]. Moreover, the peak at 1445.16 cm^{-1} was attributed to the $-CH_3$ bending vibrations, and the peaks due to a C–H stretching vibration appeared at 2951.08 cm^{-1}, it was consistent with another report [29]. The peak at 1149.01 cm^{-1} was reduced to the C–O–C symmetrical stretching vibrations of the PMMA. Besides, the adsorption peaks at 988 and 843 cm^{-1} were observed in the IR absorption spectra of the composites results from the $-CH_3$ bending wagging vibrations and the deformation vibrations of O–C–O of the PMMA [30]. The peak at 754 cm^{-1} was attributed to the puckering vibrations of the PMMA chains. The spectrum of the $Ce(OH)_2$ and Pr_2O_3 were characterized by the peaks positioned at 498 and 483 cm^{-1}, respectively [31]. These evidences indicated that PMMA was obtained by in situ polymerization of the MMA monomer. Moreover, graphite nanosheets and inorganic nanoparticles Pr_2O_3, $Ce(OH)_3$ were, together with the results of SEM and TEM micrograph, dispersed in the PMMA matrix.

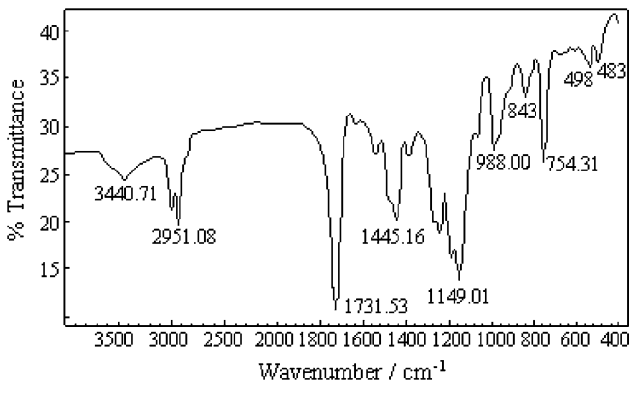

Fig. 6. FT-IR absorption spectra of the PMMA/Pr_2O_3, $Ce(OH)_3$/NanoG composite.

3.3. Thermogravimetric analysis

The TG curves (2) of PMMA/Pr_2O_3, $Ce(OH)_3$/NanoG composite was measured at heating rate of 10 °C/min, and was shown in Fig. 7. For comparison, the TG curve (1) of pure PMMA was also shown in Fig. 7. The TG curve of PMMA/Pr_2O_3, $Ce(OH)_3$/NanoG composite indicated that weight loss occurred in two steps. A reduction of sample weight was observed from 210 to 440 °C. This weight loss was attributed to burning of organic phase, the thermal dehydration of inorganic nanoparticles and the decomposition of the hydroxide precursor to form praseodymium and cerium oxide. Additional steps in weight loss was recorded in the regions 120–210 °C. This weight loss related to the evaporation of the water of chemical or physical adsorption of composite and the dissipating of no polymerization MMA monomer. No significant weight change was observed at temperatures exceeding 450 °C. The total weight loss of 88.9% at 520 °C for the composite was lower than the pure PMMA 92.64%. These results indicated that the nanosheets and inorganic nanoparticles dispersed into the PMMA matrix. The residual weight was attributed to the inorganic particles and graphite nanosheets.

For composites, the total weight loss was found to increase with increasing content of PMMA. However, more detailed investigation, currently under way, was necessary to study the composition and microstructure of the prepared composite.

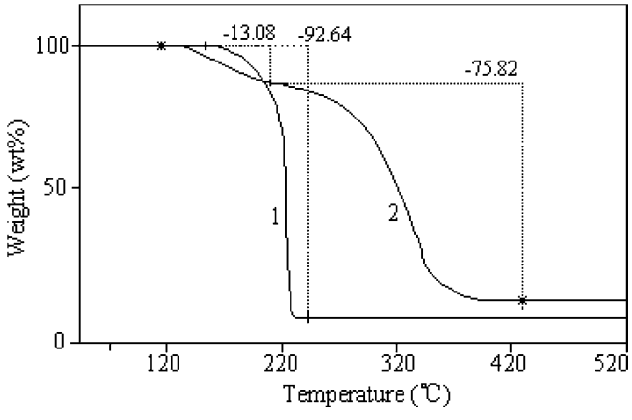

Fig. 7. TG curves of PMMA/Pr_2O_3, $Ce(OH)_3$/NanoG composite (2) and the pure PMMA (1).

It was regarded that in previous investigations [15,19], the amount of an organic phase in the composite was evaluated from thermogravimetric analysis of the composite and pure organic phase. On the other hand, further experiments had shown that phase content and crystalline of inorganic materials prepared could be influenced by PMMA [20,21,32]. It was reasonable to assume that the composite could not be considered as a simple mixture of inorganic and organic phases.

The thermal stability of composite increased with the increasing of the decomposition temperature of matrix [21]. From the TG data, it might be concluded that the thermal weight loss temperature of pure PMMA was 155 °C, but that of PMMA/Pr_2O_3, $Ce(OH)_3$/NanoG composite was 210 °C. Its indicated that the thermal stability of PMMA/Pr_2O_3, $Ce(OH)_3$/NanoG composite was increased markedly than pure PMMA. It was because that there were strong interaction between large numbers of surface atoms of Pr_2O_3, $Ce(OH)_3$ nanoparticles, graphite nanosheets and PMMA molecule chains. And the inorganic nanoparticles trammeled the movement of the PMMA molecule chains. It put the thermal decomposition of the composites at a disadvantage. Consequently the needed energy of thermal decomposition increased, namely the thermal stability of composites increased.

4. Conclusions

Graphite nanosheets were prepared by treating the expanded graphite with sonication in aqueous alcohol solution. The PMMA/Pr_2O_3, $Ce(OH)_3$/NanoG composites were prepared via in situ polymerization of MMA monomer in the presence of graphite nanosheets and $Ce(OH)_3$, Pr_2O_3 through reverse micelle template, in which the MMA was designated as oily phase. Results showed that the high-aspect-ratio structure of graphite nanosheets played an important role in forming conducting network in PMMA matrix. The thermal stability of PMMA exhibited a beneficial effect due to the introduction of graphite nanosheets and inorganic nanoparticles.

Acknowledgements

We would like to acknowledge the financial support from the National Natural Science Foundation of China (29875018), the Natural Science Foundation of Gansu Province (ZS991-A25-008-Z), Gansu Key Laboratory of Polymer Materials, the Doctorate Foundation of Northwestern Politechnical University (CX200309) and the Aeronautics Foundation of China (03H53044).

References

[1] Navarro-Laboulais J, Trijueque J, García-Jareño JJ, Vicente F. Impedance analysis of graphite/polyethylene and graphite/epoxy composite electrodes. J Electroanal Chem 1995;399(1–2):115–20.

[2] Pan QM, Guo KK, Wang LZ, Fang SB. Ionic conductive copolymer encapsulated graphite as an anode material for lithium ion batteries. Solid State Ionics 2002;149(3–4):193–200.

[3] Li WG, Johnson CL, Wang HL. Preparation and characterization of monolithic polyaniline-graphite composite actuators. Polymer 2004; 45(14):4769–75.

[4] Duquesne S, Le BM, Bourbigot S, Delobel R, Camino G. Thermal degradation of polyurethane and polyurethane/expandable graphite coatings. Polym Degrad stab 2001;74(3):493–9.

[5] Narayanan S, Schadler LS. Mechanisms of kink-band formation in graphite/epoxy composites: a micromechanical experimental study. Compos Sci Technol 1999;59(15):2201–13.

[6] Yasmin A, Daniel IM. Mechanical and thermal properties of graphite platelet/epoxy composites. Polymer 2004;45(24):8211–9.

[7] Matsuo Y, Tahara K, Sugie Y. Synthesis of poly(ethylene oxide)-intercalated graphite oxide. Carbon 1996;34(5):672–4.

[8] Du XS, Xiao M, Meng YZ, Hay AS. Synthesis and properties of poly(4,4′-oxybis(benzene)disulfide)/graphite nanocomposites via in situ ring-opening polymerization of macrocyclic oligomers. Polymer 2004;45(19): 6713–8.

[9] Xiao M, Sun LY, Liu JJ, Li Y, Gong KC. Synthesis and properties of polystyrene/graphite nanocomposites. Polymer 2002;43(8):2245–8.

[10] Shioyama H, Tatsumi K, Iwashita N, Fujita K, Sawada Y. On the interaction between the potassium-GIC and unsaturated hydrocarbons. Synth Met 1998;96(3):229–33.

[11] Wang WP, Pan CY. Synthesis and characterizations of poly(ethylene oxide) methyl ether grafted on the expanded graphite with isocyanate groups. Eur Polym J 2004;40(3):543–8.

[12] Zheng GH, Wu JS, Wang WP, Pan CY. Characterizations of expanded graphite/polymer composites prepared by in situ polymerization. Carbon 2004;42(14):2839–47.

[13] Zheng WG, Wong SC, Sue HJ. Transport behavior of PMMA/expanded graphite nanocomposites. Polymer 2002;43(25):6767–73.

[14] Ersoy OG, Nugay N. A new approach to increase weld line strength of incompatible polymer blend composites: selective filler addition. Polymer 2004;45(4):1243–52.

[15] Xiao P, Xiao M, Gong KC. Preparation of exfoliated graphite/polystyrene composite by polymerization-filling technique. Polymer 2001;42(11): 4813–6.

[16] Xiao M, Feng B, Gong KC. Preparation and performance of shape stabilized phase change thermal storage materials with high thermal conductivity. Energy Convers Manage 2002;43(1):103–8.

[17] Botti A, Pyckhout-Hintzen W, Richter D, Urban V, Straube E, Kohlbrecher J. Silica filled elastomers: polymer chain and filler characterization in the undeformed state by a SANS-SAXS approach. Polymer 2003;44(24):7505–12.

[18] Cassagnau Ph, Mélis F. Non-linear viscoelastic behaviour and modulus recovery in silica filled polymers. Polymer 2003;44(21):6607–15.

[19] Chen GH, Wu CL, Weng WG, Wu DJ, Yan WL. Preparation of polystyrene/graphite nanosheet composite. Polymer 2003;44(6): 1781–4.

[20] Chen GH, Weng WG, Wu DJ, Wu CL. PMMA/graphite nanosheets composite and its conducting properties. Eur Polym J 2003;39(12): 2329–35.

[21] Habsuda J, Simon GP, Cheng YB, Hewitt DG, Diggins DR, Toh H, et al. Sol–gel derived composites from poly(silicic acid) and 2-hydroxyethylmethacrylate: thermal, physical and morphological properties. Polymer 2002;44(17):4627–38.

[22] Du XS, Xiao M, Meng YZ, Hay AS. Direct synthesis of poly(arylene-disulfide)/carbon nanosheet composites via the oxidation with graphite oxide. Carbon 2005;43(1):195–7.

[23] Wang JJ, Zhu MY, Outlaw-Ron A, Zhao X, Manos-Dennis M, Holloway-Brian C. Synthesis of carbon nanosheets by inductively coupled radio-frequency plasma enhanced chemical vapor deposition. Carbon 2004; 42(14):2867–72.

[24] Chen GH, Weng WG, Wu DJ, Wu CL, Lu JR, Wang PP, et al. Preparation and characterization of graphite nanosheets from ultrasonic powdering technique. Carbon 2004;42(4):753–9.

[25] Fukuda K, Kikuya K, Isono K, Yoshio M. Foliated natural graphite as the anode material for rechargeable lithium-ion cells. J Power Sources 1997; 69(1–2):165–8.

[26] Kuang Q, Xie SY, Jiang ZY, Zhang XH, Xie ZX, Huang RB, et al. Low temperature solvothermal synthesis of crumpled carbon nanosheets. Carbon 2004;42(8–9):1737–41.
[27] Chen SC. Important inorganic chemistry reaction. vol. 2. Shanghai: Shanghai Technology Press; 1963 p. 864 [see also p. 703].
[28] Hamwi A, Marchand V. Some chemical and electrochemical properties of graphite oxide. J Phys Chem Solids 1996;57:867–71.
[29] Matsuo Y, Kume K, Fukutsuka T, Sugie Y. Electrochemical hydrogenation of carbon from pyrolysis of graphite oxide. Carbon 2003;41(11):2167–70.
[30] Lu WM, Shao ZP, Chen WG, Hu JB, Luo XY, Dong N. Synthesis and characterization of the complexes of rare earth with α-methylacrylic acid. J Hangzhou Univ 1996;24(3):251–5.
[31] Kazuo N. Infrared and Raman spectra of inorganic and coordination compounds. vol. 2. Beijing: Chemical Industry Press; 1991 p. 125.
[32] Pötschke P, Fornes TD, Paul DR. Rheological behavior of multiwalled carbon nanotube/polycarbonate composites. Polymer 2002;43(11): 3247–55.